Rossby Wave Breaking, Microbreaking, Filamentation, and Secondary Vortex Formation: The Dynamics of a Perturbed Vortex

L. M. POLVANI

Department of Applied Physics, Columbia University, New York, New York

R. ALAN PLUMB

Center for Meteorology and Physical Oceanography, Massachusetts Institute of Technology, Cambridge, Massachusetts

(Manuscript received 18 February 1991, in final form 27 June 1991)

ABSTRACT

The behavior of an isolated vortex perturbed by topographically forced Rossby waves is studied using the method of Contour Dynamics. For a single-contour vortex a distinct forcing threshold exists above which the wave breaks in a dynamically significant way, leading to a disruption of the vortex. This *breaking* is distinguished from the process of weak filamentary breaking described by Dritschel and classified here as *microbreaking;* the latter occurs in nondivergent flow even at very small forcing amplitudes but does not affect the vortex in a substantial manner. In cases with finite Rossby deformation radius (comparable with the vortex radius) neither breaking nor microbreaking occurs below the forcing threshold. In common with previous studies using high-resolution spectral models, the vortex is not diluted by intrusion of outside air, except during remerger with a secondary vortex shed previously from the main vortex during a breaking event. The kinematics of the breaking process and of the vortex interior and the morphology of material ejected from the vortex are described. When the Rossby radius is finite there is substantial mixing in the deep interior of the vortex, even when the vortex is only mildly disturbed. Implications for the stratospheric polar vortex are discussed.

1. Introduction

Our perception of the dynamics of the wintertime stratosphere changed profoundly with the demonstration by McIntyre and Palmer (1983) that the large-amplitude, quasi-stationary Rossby waves, propagating upward along the edge of the polar vortex, can and do break, thus ejecting material from inside the vortex and mixing some or all of it into the midlatitude air. At about the same time, the onset of ozone depletion within the springtime Antarctic vortex and, to a lesser extent, within the Arctic vortex gave new urgency to the study of the dynamics of, and the transport of trace species in, these systems. A discussion of some of the issues thus raised may be found in Juckes and McIntyre (1987), McIntyre (1987, 1989), Anderson et al. (1991), Schoeberl and Hartmann (1991), and Schoeberl et al. (1991).

Some of the key questions are the following. First, to what extent is the air inside the vortex isolated from incursions of midlatitude air? This question is of considerable importance to our understanding of the chemistry of the vortex. In some such calculations (e.g., Anderson et al. 1989) it is assumed that the polar vortices are "containment vessels" (Juckes and McIntyre 1987) within which constituent budgets are unaffected by admixture of midlatitude air; others (e.g., Proffitt et al. 1989, 1990) have argued that material is exchanged inward and outward across the vortex edge.

Second, under what conditions is air ejected from the vortex (i.e., under what conditions do Rossby waves break) and what is the morphology of the breaking (does it form thin filaments or is air ejected in large-scale, secondary vortices, or both)? In principle, transport of the anomalous polar chemistry into the sunlit midlatitudes could bring about significant ozone depletion there. If the vortex air is ejected in thin filaments, interaction with midlatitude air could neutralize the chemical activity very quickly (Prather and Jaffe 1990) but longer-lasting effects could take place if ejection occurs on larger scales.

Satellite observations do little to resolve these questions, because of their limited resolution; thin features would either appear smoothed out in the analysis or would be missed altogether. Aircraft measurements taken during the Airborne Antarctic Ozone Expedition (see especially the sections near the vortex edge shown in Anderson et al. 1989) do appear to show the presence of finescale structures.

Corresponding author address: Dr. Lorenzo M. Polvani, Department of Applied Physics, Seeley W. Mudd Bldg., Room 209, Columbia University, New York, NY 10027.

Because of the coarse resolution of satellite radiance measurements and the consequent limited data quality inherent in global stratospheric analyses, much of the recent progress in our understanding of polar vortex dynamics has come from high-resolution modeling studies (Juckes and McIntyre 1987; Juckes 1989; Salby et al. 1990). These studies have shown the erosion of the vortex through the effects of breaking Rossby waves, the isolation of the vortex (i.e., the impermeability of the vortex edge to inward-moving, but not outward-moving, air) under simple conditions, the steepening of potential vorticity gradients to produce a sharp vortex edge, and the effects of thermal relaxation in mitigating the dynamical tendency to erode the vortex. Above all, perhaps, they have also illustrated the complex behavior of products of the Rossby wave breaking process and of the flow evolution even in highly simplified experiments. The relative expense of running conventional models at the required high resolution precludes, however, the methodical sweep of parameter space that might help to elucidate this complexity.

The approach we have taken here is to model the dynamics of simple vortices, perturbed by quasi-stationary, topographically driven Rossby waves, using the method of Contour Dynamics/Contour Surgery (CD/CS: see Dritschel 1989a for an extensive review) applied to a quasigeostrophic shallow-water system. We consider the simplest possible analog of the winter stratosphere, invoking an f-plane fluid system comprising, in its undisturbed state, a circular vortex of uniform potential vorticity Q surrounded by an infinite region of uniform and lower Q. All the potential vorticity gradient is thus concentrated at the vortex edge. We must further neglect diabatic and frictional effects, so that Q is a conservative quantity; the evolution of such a system is then entirely described by the evolution of the contour separating the regions of different Q. The two-dimensional problem thus reduces to the one-dimensional one of following the potential vorticity interface, enabling very high resolution to be achieved with modest computing resources.

A simplified system such as that studied here is not intended to be a model of the stratospheric polar vortex. For one thing, the geometry is wrong, which means that the relationship between Q and the geostrophic flow differs from that appropriate to the sphere. Nevertheless, we do take care to reproduce one of the most important characteristics of the zonal flow in the winter stratosphere—the existence of the subtropical zero wind line separating midlatitude westerlies from tropical easterlies. We do this by choosing the value of Q outside the vortex in such a way as to ensure that there is a realistic reversal of the unperturbed flow there. Second, the specification of a piecewise continuous potential vorticity distribution is highly idealized; nevertheless, the stratospheric vortex in midwinter is indeed characterized by a sharp isentropic gradient of potential vorticity at the vortex edge with relatively weak gradients elsewhere (McIntyre and Palmer 1983). The dynamical system defined by the single contour vortex does not, however, represent the observed strong gradient of potential vorticity in the tropics. Third, those effects associated with nonconservative processes, especially diabatic heating, cannot be represented in the model. This restriction limits us to the short-term dynamical processes that are the focus of this work. What we hope to achieve in this study is a deeper understanding of the complex nonlinear dynamics of a simple perturbed vortex, which we see as a necessary precursor to understanding the more complex stratospheric problem.

The formulation of the modeled system is discussed in section 2. In section 3 we present a general discussion of the varied behavior we find in these experiments; if the topographic amplitude is sufficiently large, the forced Rossby wave breaks, ejecting vortex material outward. More details of the results are given in section 4, where we discuss the critical amplitude for the onset of wave breaking (and the distinction between this process and the finescale "microbreaking" found for nondivergent flow at subcritical forcing amplitudes); the nature of material ejected from the vortex during breaking (whether filaments or secondary vortices); our confirmation of earlier model results showing the absence of incursion of outside material into the vortex, except during remerger of the parent vortex with a secondary vortex; and the kinematics of tracer transport inside and outside the vortex in both breaking and nonbreaking cases. The results are summarized and their applicability to the stratosphere discussed in section 5.

2. Formulation of the model

We consider quasigeostrophic motion in a shallow-water system with rotation rate $0.5f_0$, mean depth D, and total depth $D - h$, where the bottom topography h is small compared to D. Defining γ to be the inverse Rossby deformation radius, that is, $\gamma = f_0/\sqrt{gD}$, the quasigeostrophic potential vorticity is

$$Q = f_0 + \nabla^2\psi - \gamma^2\psi + f_0\frac{h}{D}, \tag{1}$$

where ψ is the geostrophic streamfunction.

The unforced basic state is chosen to be a single contour vortex, with potential vorticity distribution

$$Q = \begin{cases} Q_i, & \text{if } r < r_0 \\ Q_o, & \text{if } r > r_0; \end{cases} \tag{2}$$

thus, Q_i and Q_o are the absolute vorticities inside and outside the vortex edge located at $r = r_0$. The corresponding velocity distribution is

$$v = r_0(f_0 - Q_o)V(r) \tag{3}$$

where

$$V(r) = \begin{cases} \rho I_1(\gamma r)K_1(\gamma r_0) - \dfrac{1}{\gamma r_0} I_1(\gamma r), & \text{if } r < r_0 \\ \rho K_1(\gamma r)I_1(\gamma r_0) - \dfrac{1}{\gamma r_0} I_1(\gamma r), & \text{if } r > r_0 \end{cases} \tag{4}$$

with $\rho = (Q_i - Q_o)/(f_0 - Q_o)$ and I_1 and K_1 modified Bessel functions in the usual notation.

We confine attention to cyclonic vortices, $Q_i > f_0$. In order to ensure the existence of a reversal in the circulation at some finite radius (as an analog of the stratospheric zero-wind line), we must have $Q_o < f_0$. An inevitable consequence of insisting on a circulation reversal with a single-contour vortex is that the anticyclonic circulation becomes infinite at infinite radius. However, since all the dynamics is concentrated at the contour, the flow at very large r (beyond the maximum radius to which the contour extends during its evolution, typically $r = 3r_0$ in active cases) is of no importance to the dynamics of the problem.

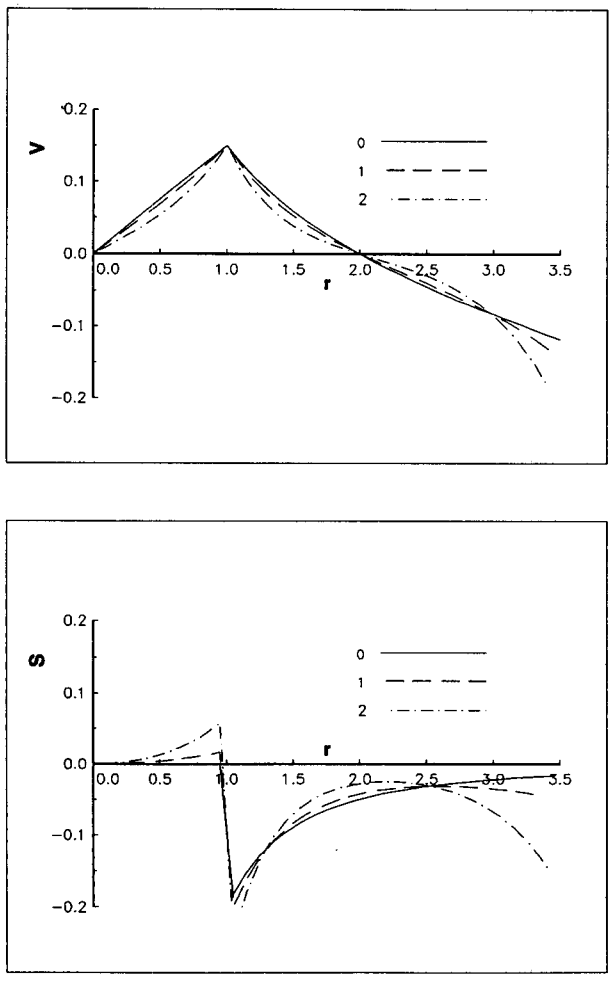

FIG. 1. Structure of the undisturbed vortex. Upper panel: velocity profiles (V is in units of $r_0 f_0$, r in units of r_0). Lower panel: strain rate $S = (r/2)d(v/r)/dr$ (in units of f_0). Curve labels are values of γr_0, where γ is the inverse Rossby deformation radius.

TABLE 1. Parameter values used for the runs presented in the paper. The surgery parameter δ was chosen to be 0.00125, except where indicated otherwise.

Figure	Q_i/f_0	Q_o/f_0	H_0	γr_0
2	1.300	0.900	0.15	0.0
3	1.300	0.900	0.18	0.0
4	1.363	0.942	0.20	0.5
5	1.300	0.900	0.20	0.5
6	1.681	0.997	0.20	2.0
8	1.300	0.900	0.15	0.0
10	1.300	0.900	0.25	0.0
13	1.300	0.900	0.12	0.0
14	1.300	0.900	0.17	0.0
15	1.300	0.900	0.25	0.0

For the nondivergent, barotropic case, we take $(Q_i, Q_o) = (1.3, 0.9) \times f_0$, which results in a velocity profile shape labeled "0" in Fig. 1. The first number fixes the vortex strength, and the second gives a zero-wind line at $r = 2r_0$; the maximum velocity occurs at the vortex edge, and its value is $0.15 r_0 f_0$. (In dimensional terms, this corresponds to about 65 m s^{-1} for a vortex radius of 3000 km.) For divergent cases, that is, nonzero γ, we cannot hold fixed both the distribution of potential vorticity and the velocity profile (and we are of course obliged to maintain the shape of the initial Q distribution, which in turn limits our ability to control the details of the velocity distribution). Fixing Q_i and Q_o leads to velocity profiles that vary greatly with γ. Except where otherwise noted, values of Q_i and Q_o were therefore chosen so as to fix the circulation at the vortex edge ($v = 0.15 r_0 f_0$ at $r = r_0$) and the radius of the flow reversal ($v = 0$ at $r = 2r_0$). The actual potential vorticity values are then determined from (4), and are listed in Table 1. The undisturbed velocity profiles (shown in Fig. 1) then vary relatively little with γ; one difference that turns out to be important (as will become apparent later) is the stronger shear beyond the flow reversal for $\gamma > r_0^{-1}$.

This circular vortex is perturbed by a bottom topography $h(r, \theta)$, which we choose to be of the form

$$h(r, \theta) = DHJ_1(\kappa r)\cos\theta, \tag{5}$$

with $\kappa = 1.6 r_0^{-1}$ and where D is the fluid depth. Thus, the topography comprises wavenumber 1 in azimuth, with the first peak/trough at radius $1.14 r_0$, just outside the undisturbed vortex edge. The second, weaker peak/trough is at radius $3.33 r_0$, which is far enough away from the undisturbed vortex not to have substantial impact on the dynamics unless the vortex is grossly disturbed. The variable parameter in (5) is the dimensionless measure H of the topographic height.

The topography is introduced smoothly by specifying $H = H(t)$, where

$$H(t) = H_0(1 - e^{-t/\tau}), \tag{6}$$

where $\tau = 2.5$ d for most experiments. For $t \gg \tau$, therefore, the topographic forcing is sustained at a constant amplitude.

The reason for choosing the functional form given in (5) for the forcing h is the simplicity it affords in the calculation. Topographic forcing preserves conservation of potential vorticity (1) and so the evolution of Q is completely determined by advection of the potential vorticity contour. In order to move the contour, we need to compute the velocity at the contour, given its current position. Thus, (1) must be inverted for ψ. This is done by writing

$$\psi = \psi_v + \psi_f \tag{7}$$

where ψ_v is the vortex component and ψ_f is the component due to the forcing. These must satisfy, respectively,

$$\nabla^2\psi_v - \gamma^2\psi_v = Q - f_0 = \begin{cases} Q_i - f_0, & \text{inside} \\ Q_o - f_0, & \text{outside} \end{cases} \tag{8}$$

where "inside" and "outside" refer to the regions inside and outside the potential vorticity contour, and

$$\nabla^2\psi_f - \gamma^2\psi_f = -f_0\frac{h}{D}. \tag{9}$$

The vortex component ψ_v defined as the solution of (8) is calculated using the usual CD method. Specifically, the corresponding Cartesian velocity components u_v and v_v are given by (see, e.g., Polvani et al. 1989a):

$$[u_v, v_v](\mathbf{x}) = (2\pi)^{-1}(Q_o - Q_i) \times \oint G(|\mathbf{x} - \mathbf{x}'|)[-dx', dy'] \tag{10}$$

where the integrals are along the contour and where the Green function is

$$G(r) = -K_0(\gamma r). \tag{11}$$

The additional component ψ_f associated with the topographic forcing is obtained directly by solving (9):

$$\psi_f = \frac{f_0 H}{(\kappa^2 + \gamma^2)} J_1(\kappa r)\cos\theta. \tag{12}$$

This contribution to the velocity at the vortex edge can thus be determined analytically, since

$$u_f = -\frac{\partial\psi_f}{\partial y}, \quad v_f = \frac{\partial\psi_f}{\partial x}. \tag{13}$$

The algorithms we have used for the discrete representation of the contours, the numerical evaluation of the contour integrals, and time stepping of the solution are those of Contour Surgery, and are described in detail in Dritschel (1989a). Contour Surgery also provides for the automatic removal (surgery) of filaments that are smaller than a given scale δ. For reference, most of the runs presented here were performed with $\delta = 0.00125 \times r_0$ (except for a few that were done at higher resolution, i.e., smaller δ). This choice of δ implies that, for a typical value of $r_0 = 3000$ km, the unresolved scales are smaller than 3.75 km.

Many experiments were performed at several values of γ in the range $0 \leq \gamma \leq 2r_0^{-1}$ and for different values of H_0. The behavior of the disturbed vortex over this parameter range is first illustrated by the examples presented below, while detailed discussion of specific issues is given in section 4. (The specific parameter values used in the runs presented in the paper are given in Table 1.)

3. Results: General characteristics

In this section, in order to introduce the reader to the general characteristics of vortex behavior revealed by these experiments, we present an overview of our results. More detailed discussion of specific characteristics and dynamical interpretation is given in section 4.

Evolution of Q in two contrasting nondivergent experiments is shown in Figs. 2 and 3. For the weaker forcing, $H_0 = 0.15$ (Fig. 2), the vortex remains intact. The direct effect of the forcing (which would be pre-

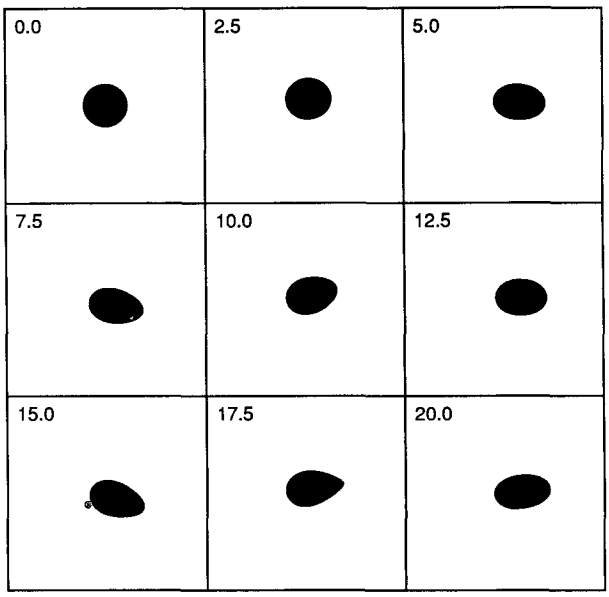

FIG. 2. Evolution of the vortex edge for the standard barotropic case ($\gamma = 0$) with $H_0 = 0.15$. Each box is centered on the coordinate origin (the center of the undisturbed vortex) which is indicated by the small cross. The numbers in the upper left-hand corner of each box gives the time in days.

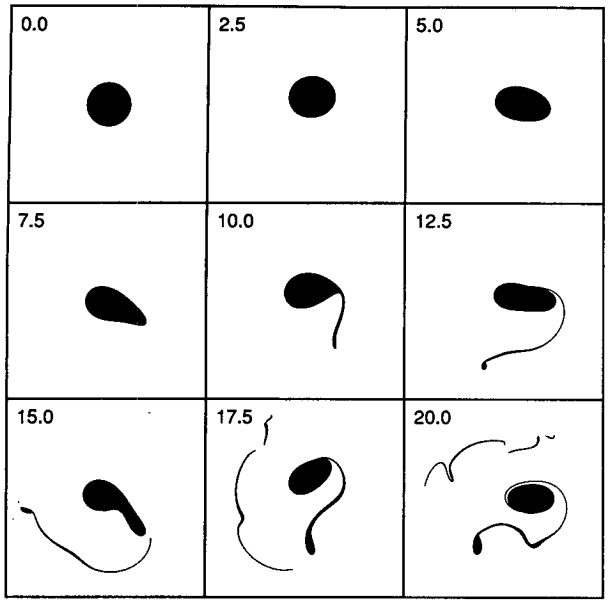

FIG. 3. As Fig. 2, but for larger forcing amplitude: $H_0 = 0.18$.

dicted by linear theory) is simply to excite stationary and transient wave 1 Rossby waves on the vortex edge. (Since there is no dissipation mechanism operating in this case—no fine scales are generated so the surgery algorithm is not invoked—and no potential vorticity gradient beyond the vortex edge to permit leakage of wave activity, the transients excited by the introduction of the forcing cannot decay by linear processes.) The amplitudes of the stationary and transient components are comparable, and the net effect is of a fluctuating wave 1, with period of between 10 and 12 d; according to linear theory, the period of the free wave 1 mode on this vortex is 10 d. Nevertheless, the effects of nonlinearity are considerable at this amplitude. In particular, it is noteworthy that the displacement of the edge departs considerably from a smooth sinusoid, periodically forming a localized region of high curvature (e.g., at $t \approx 17.5$ d). In light of what follows, this behavior appears to herald the onset of breaking of the Rossby wave and subsequent loss of integrity of the vortex; the present case is in fact just subcritical and so no breaking occurs. (It will be shown below, on the basis of experiments run longer and at higher resolution, that this statement has to be qualified.)

At a slightly increased forcing amplitude, breaking does indeed occur near the high-curvature region. Figure 3 shows the response to $H_0 = 0.18$. Around $t = 8$ d, a region of high curvature forms, evolving into a thin filament of vortex material that is ejected into the surrounding fluid. This soon becomes so thin that it is cut off by the surgery and becomes an isolated filament orbiting the vortex. Several such "events" then follow at intervals of approximately 8 days. Close inspection of the vortex evolution reveals that each breaking event generates a transient disturbance that propagates "eastward" around the vortex edge and, on completing one complete circuit of the vortex, triggers the next event. In some events the ejected tongue of vortex material is initially relatively thick, though it quickly becomes stretched and thinned. This latter process appears to occur most rapidly at the vortex end of the filament and most slowly at the free end. Eventually, after several more breaking events, the vortex is torn apart. Increasing H_0 beyond 0.18 produces similar behavior, though the time scales of breaking and of vortex destruction are reduced. Somewhat different long-term behavior was found for divergent cases with $\gamma \geq r_0^{-1}$; in many of these cases the wave breaking stopped after one or two events, and (at least over the period of the integrations) the vortex was not ultimately destroyed.

The detailed evolution of the material ejected during events was found to vary somewhat depending on the configuration of the initial flow. For example, Fig. 4 shows the a case with $\gamma = 0.5r_0^{-1}$ (i.e., Rossby radius equal to the diameter of the initial vortex) and $H_0 = 0.20$. Here, rather than ejecting a thin filament, the vortex elongates ($t = 9$ d) and ejects a secondary vortex. The deformation flow close to the point of separation ($t = 9$–15 d) stretches the "tail" of this secondary vortex and thins it out to the point that it becomes truncated. Subsequently, the vortex at the head of the ejected material rolls up and separates from the filament, which itself becomes strongly deformed. At later times, the remnant of the original vortex and the substantial secondary vortex orbit each other anticyclonically, before merging together to re-form the main vortex. This latter behavior will be discussed in more detail in the next section.

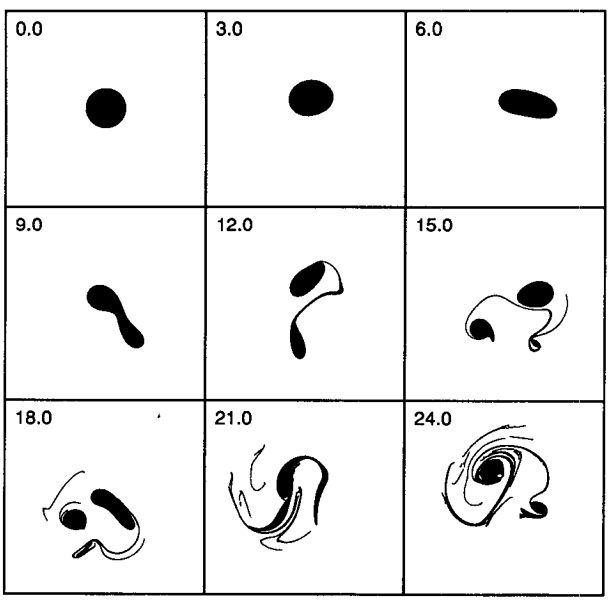

FIG. 4. As Fig. 2, but for $\gamma = 0.5r_0^{-1}$ and $H_0 = 0.20$.

One question of interest to us in this study was to investigate whether, as was found in previous studies (Polvani et al. 1989a; Waugh and Dritschel 1991), the roll-up of vorticity filaments is favored at finite γ. Although this appears to be the case in the example just described, such behavior was not generally observed in these experiments. This is illustrated by a comparison of Fig. 4 with Fig. 5, the latter showing another case with $\gamma = 0.5r_0^{-1}$ and $H_0 = 0.20$ but with the potential vorticity values the same as the nondivergent case (so that, in this case, the flow reversal is no longer at $r = 2r_0$). Thus, the two cases have the same value of γ, but different initial states. In the latter case, however, as Fig. 5 clearly shows, ejection of vortex material occurs as a continuous stream into a single strand of material (such behavior was found to be common for nonzero γ) until, by day 20, the original vortex is almost exhausted of material. The lifetime of this filament is quite long, compared with the nondivergent case; nevertheless, a strong waviness develops along the filament around $t \approx 10 - 15$ d, which ultimately leads to an extremely convoluted potential vorticity structure outside the main vortex.

An even more extreme example of filament longevity is shown in Fig. 6, for which $\gamma = 2.0r_0^{-1}$ (Rossby radius one-half of the initial vortex radius) with standard values of Q_i and Q_o (cf. Table 1) and with $H_0 = 0.2$. Like the case of Fig. 5, vortex material is ejected continuously in a single filament, which is now so stable that the strong "westward" flow wraps it several times around the main vortex.

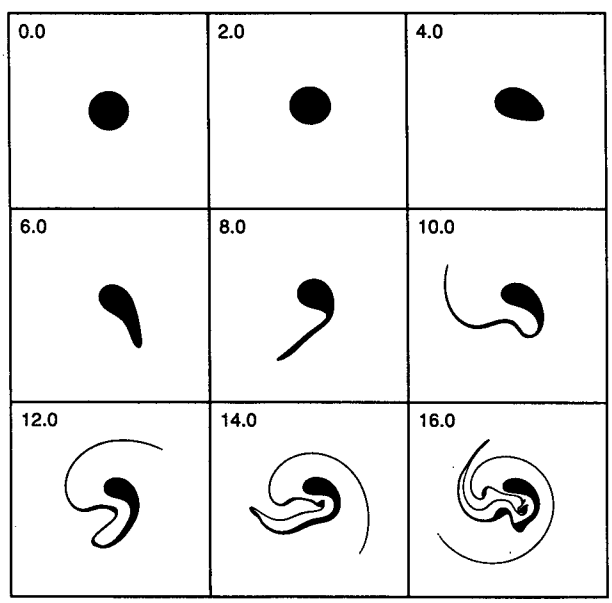

FIG. 5. As Fig. 2, but for a nonstandard initial condition (see text) with the same parameters as those of Fig. 4, i.e., $\gamma = 0.5r_0^{-1}$ and $H_0 = 0.20$.

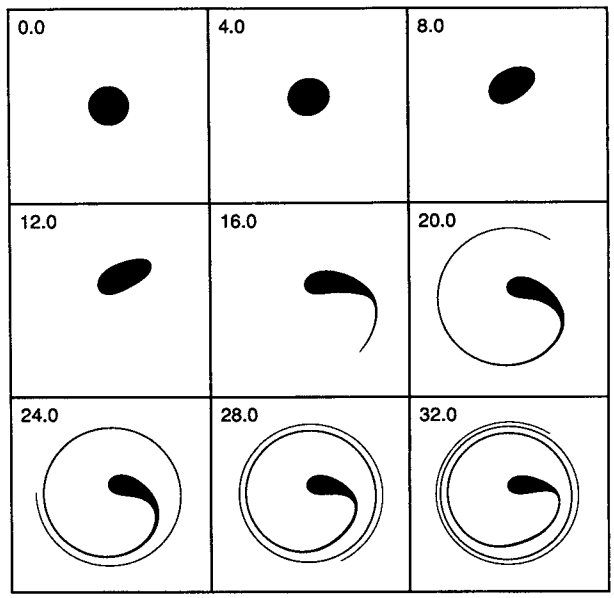

FIG. 6. As Fig. 2, but for $\gamma = 2.0r_0^{-1}$ and $H_0 = 0.20$.

4. Discussion

a. *The onset of breaking*

As the nondivergent cases of Figs. 2 and 3 show, there is a critical magnitude of the forcing required to initiate wave breaking on the edge of a single-contour vortex. With subcritical forcing, no breaking occurs in these experiments; fluid particles on the vortex edge undergo displacements that are apparently reversible (although the vortex edge becomes increasingly nonsinusoidal as the breaking threshold is approached). In fact, the development of strong curvature as a herald of the onset of breaking parallels the well-known situation of almost-breaking surface gravity waves (e.g., Banner and Phillips 1974).

Polvani et al. (1989b) found that, in the case of elliptical vortices perturbed with an unstable normal mode, the onset of filamentation is associated with the existence of a stagnation point in the corotating flow (i.e., relative to a rotating frame of reference in which the vortex is quasi steady) coinciding with the contour. If transients are neglected, the flow is steady and simple kinematics (together with the weakness of the locally induced contribution to the velocity field) then leads to the expectation that vortex material will be pinched off at this point—outward, in the usual case where the stagnation point is outside the vortex.

The present cases may be viewed in the same light; here the forced component of the disturbance (as opposed to the transients excited by the switch-on; the possible effects of these will be discussed below) is stationary and the relevant frame of reference is the stationary one. In the absence of forcing, the vortex is of

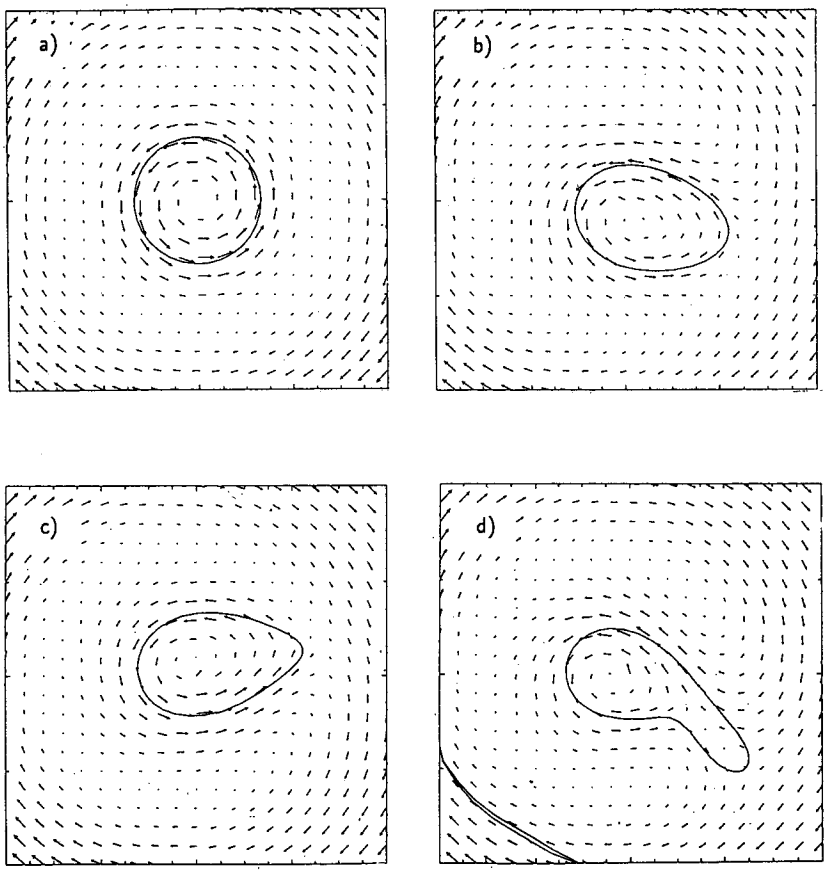

FIG. 7. The velocity field around the perturbed vortex for the case shown in Fig. 2: (a) the undisturbed vortex at $t = 0$; (b) the flow at $t = 7.5$d; (c) $t = 17.5$. (d) Flow at $t = 15$d for the case shown in Fig. 3. Note the location of the stagnation points.

course circular and the stagnation "point" is the circle of no motion at $r = 2r_0$, as illustrated in Fig. 7a. For small wave amplitude, the vortex edge distorts; outside the vortex an anticyclone is centered near $\vartheta = \pi$ (i.e., near the valley in the topography) and a stagnation point is located near $\vartheta = 0$, inside the undisturbed circle of no motion but outside the vortex near its outermost extension. This is illustrated in Fig. 7b, which shows the flow at an early stage of evolution for the case of Fig. 2. (The anticyclone corresponds to the "cat's eye" familiar from the nonlinear theory of Rossby wave critical layers, e.g., Stewartson 1978; Warn and Warn 1978; Haynes 1989.) With larger, but still subcritical, wave amplitude, the stagnation point moves closer to the edge (Fig. 7c). Finally, in supercritical cases (Fig. 7d), the stagnation point moves inside the vortex and breaking occurs.

In fact, linear calculations predict that the contour meets the stagnation point for $H_0 = 0.217$. The experiments previously described (and shown in Figs. 2 and 3) give breaking onset at a value of H_0 about 25% less than this. There could be several reasons for this difference. One—suggested by the obvious departures from linearity of the perturbation to the vortex edge in Fig. 2—is simply that the dynamics is far from linear at forcing amplitudes near breaking. A second possible reason is that the presence of the transients superposed on the stationary forced wave will at times increase the amplitude of the edge displacement, and thus facilitate breaking at lower forcing amplitudes. However, this was tested by comparing the results shown in Fig. 3 with results from another experiment, identical except that the "switch-on time" τ was increased to 12.5 d (from 2.5 d). This resulted, as expected, in a much reduced transient component of the flow. Nevertheless, breaking still occurred; it was delayed (first appearing at $t \approx 35$ d, rather than 10 d) but subsequent evolution of the vortex was qualitatively little different from that of the original experiment. Thus, at least in this case, the transients appear to have made little impact on the occurrence or otherwise of breaking.

b. Microbreaking at subcritical forcing

While the onset of breaking is sudden (with respect to H_0) and apparently clear-cut, higher-resolution ex-

periments for nondivergent flow ($\gamma = 0$) reveal that the vortex does in fact lose very small amounts of material even when the forcing is subcritical with respect to the breaking threshold. This is illustrated in Fig. 8, which shows typical behavior in such cases (the parameters here are identical to the ones in Fig. 2, except for the cutoff scale δ, which is much smaller here). After some time (typically much longer than the time for breaking in supercritical cases) a small region of high curvature forms on the vortex from which a very thin filament is shed. This phenomenon falls under McIntyre and Palmer's (1984, 1985) definition of "breaking": there is irreversible deformation of the dynamically relevant material contours that, in this case, comprise our single potential vorticity contour. However, there are several reasons to distinguish this from the behavior associated with Rossby wave breaking as seen in the stratosphere and as previously discussed; for this reason we classify it somewhat differently. Given the extreme thinness of the ejected filament, the term "microbreaking" seems appropriate.

For one thing, this subcritical behavior always generates extremely thin filaments that contain very small amounts of material (the thickness of the filament being about one-thousandth of the original vortex radius for the case in Fig. 8). In Fig. 9 (for $\gamma = 0$) we quantify the effect of this subcritical microbreaking as opposed to supercritical breaking by plotting the diagnostic quantity $\Sigma \equiv \langle r^2 \rangle - \langle r \rangle^2$, where angle brackets denotes the area-weighted average of all material originally within the circular vortex. For the supercritical breaking cases, $H_0 \geq 0.16$, breaking is manifested by a clear and sudden tendency for Σ to increase with time. No such tendency is evident in the subcritical cases; even after the onset of filamentation Σ does not show any noticeable increase, indicating the very small amounts of vortex material within the extruded filaments.

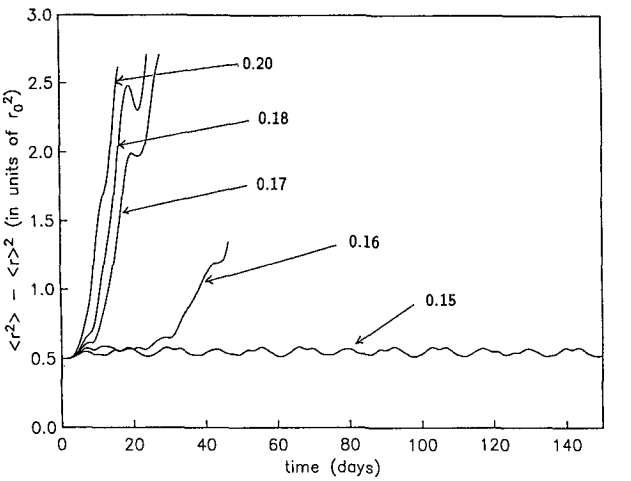

FIG. 9. Evolution of the diagnostic Σ (see text) for breaking and nonbreaking nondivergent ($\gamma = 0$) cases. Labels on curves are values of H_0.

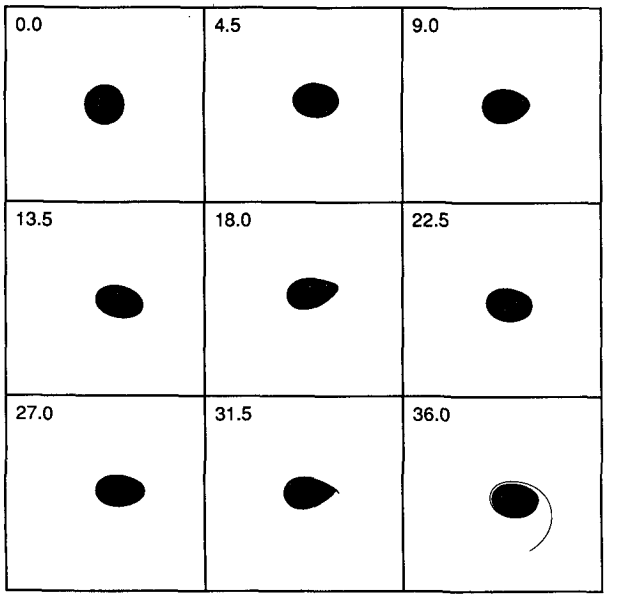

FIG. 8. As Fig. 2, but at higher resolution ($\delta = 5.0 \times 10^{-5}$).

Second, we find that microbreaking vanishes suddenly for all subcritical forcing as the resolution of the model is degraded. If the process were simply a progressively weaker form of breaking as H_0 decreases, one would expect that the breaking transition would decrease steadily with increasing resolution. However, we have found that the critical amplitude for breaking is quite insensitive to the resolution.

Third, onset of microbreaking is slow compared with supercritical breaking. The case of Fig. 8 breaks at $t \approx 30$ d, whereas, as Fig. 9 shows, supercritical breaking typically occurs within 10 d (the marginally supercritical case $H_0 = 0.16$ being slower, however).

This subcritical behavior appears to be a manifestation of the "filamentation" phenomenon noted by Deem and Zabusky (1978) and extensively studied by Dritschel (1988). Unlike the supercritical breaking case, where linear theory predicts a stagnation point near the contour, the formation of high curvature in these subcritical cases (or, equivalently, the appearance of a stagnation point near the vortex edge) that precedes filamentation is localized and seems to result from the slow accumulation of nonlinearities in the Rossby wave.

We have not found microbreaking in divergent cases with γ nonzero. For example, an experiment with the same resolution as that shown in Fig. 8 but with $H_0 = 0.11$ at $\gamma = r_0^{-1}$ reveals no irreversible buckling of the potential vorticity contour during the 250-day run.

Of course we cannot rule out the possibility that microbreaking will occur at later times or in a model with even higher resolution. However, we have run our model to a much finer resolution than that at which microbreaking first occurs in the nondivergent case. Therefore, it is our impression that microbreaking is entirely suppressed in the presence of finite Rossby radius (consistent with earlier findings of Polvani et al. 1989a and Dritschel 1989a).

c. *Filament and secondary vortex formation*

The experimental results, some of which have been described here, reveal a wide range in the behavior of vortex material ejected into the outer region. At the time of ejection, the material may be in the form of a filament (e.g., Fig. 3 at $t = 10$ d) or a thick secondary vortex (Fig. 4; $t = 12$ d). Subsequently, a filament may be stretched out ever thinner until lost to the calculation (Fig. 3; 10–15 d) or, more frequently, roll up into one or more discrete vortices (Fig. 5). A secondary vortex, once formed, usually maintains its identity but frequently leaves behind a filamentary tail (Fig. 4). At least some of these characteristics appear to have simple explanations.

In the initial stages of ejection during a wave-breaking event, the morphology of the ejected material depends on the supercriticality of the flow with respect to the wave-breaking criterion. With weak supercriticality, the breaking is filamentary, at least in the early stages (Fig. 3); when perturbed more strongly, however, the ejecta are more bulky, as shown in Fig. 10 (the only difference from the case in Fig. 3 being the larger value of forcing amplitude H_0). In the terminology used above, it seems that for small supercriticality the stagnation point is located close to the vortex edge, thus pinching off a thin filament; for larger supercriticality the stagnation point moves well inside the edge, thus pinching off a more substantial amount of vortex material. The distinction is illustrated schematically in Fig. 11.

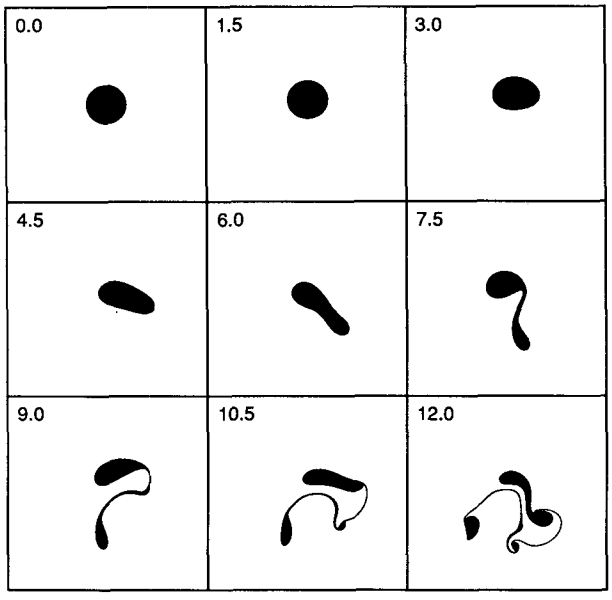

FIG. 10. As Fig. 2, but for $H_0 = 0.25$.

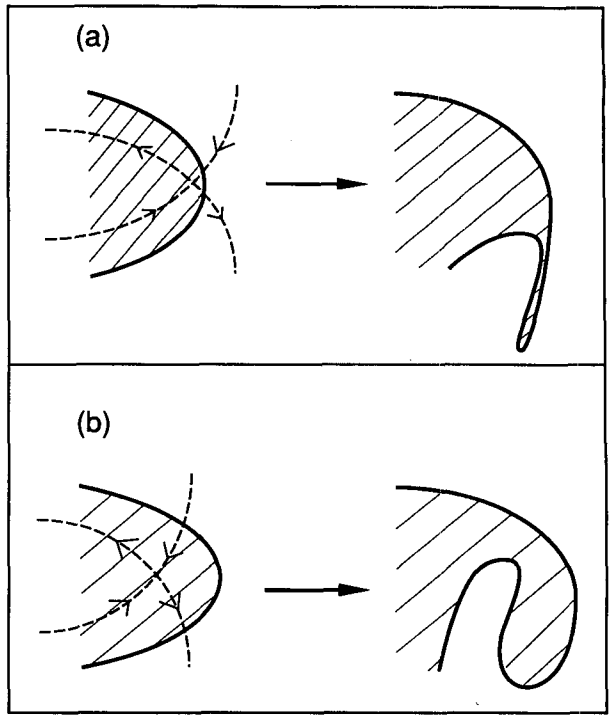

FIG. 11. Schematic illustrating the kinematics of wave breaking at the vortex edge. (a) Weakly supercritical case, with stagnation point close to vortex edge and ejection of a thin filament. (b) Strongly supercritical case with stagnation point well inside the vortex and ejection of a greater bulk of vortex material.

Once outside the vortex, the fate of the ejected material depends on the deformation field there. In most cases filaments ejected from the vortex are disrupted through the appearance of wavy disturbances, which frequently roll up into discrete secondary vortices. Indeed, this is just what would be expected for an isolated filament; since the sign of the potential vorticity gradient is necessarily of opposite sign on the two edges, parallel flow theory leads us to anticipate the appearance of just such wavy disturbances through instability of the filament. This being the case, the longevity of filaments in some cases—Fig. 6 showing one of the more dramatic examples—is the more remarkable. The reason for this appears to be that demonstrated by Dritschel (1989b), namely, that the filaments are stabilized by the flow field of the main vortex. In the pres-

ence of sufficiently strong "adverse shear" (i.e., an externally controlled shear with the opposite sense as and equal or greater magnitude than that produced by the filament's potential vorticity alone) the filament is linearly stable. In the case of Fig. 6, the shear is indeed found to be adverse in this sense. Note, however, the arguments of Dritschel et al. (1991), who show that a filament can also be stabilized by a very small pure strain; it is difficult to separate the two effects in our results.

This phenomenon of long-lived filaments was found primarily in the experiments with $\gamma \geq r_0^{-1}$. The reason for this appears not to be intrinsic to the dynamics of flow with finite Rossby deformation radius, but rather a property of the undisturbed vortex flow in these experiments. At the larger values of γ (see Fig. 1) the anticyclonic shear outside the vortex becomes increasingly strong beyond the "zero wind line" at $r = 2.0r_0$ (cf. the large values of the strain rate S at large r for $\gamma = 2r_0^{-1}$). It is this background shear that stabilizes the filaments ejected into it.

FIG. 12. An enlargement of the last frame of Fig. 4, showing entrainment of outer fluid (white) into the vortex (black) after "remerger."

d. *Robustness of the vortex to intrusion of outside material*

It is clear from what we have presented thus far that results of these experiments confirm the "onesidedness" noted from other approaches (especially Juckes and McIntyre 1987), namely, that ejection of vortex material is not accompanied by injection of outside fluid. This statement is evident in all cases illustrated herein thus far. The reason appears to be the asymmetry of the large-scale strain field with respect to the vortex edge. This asymmetry is imposed by the "background" unperturbed vortex flow; the structure of the strain in the undisturbed flow is shown in Fig. 1. The contrast between the inside of the vortex and the region just outside is obvious. A perturbation on the vortex edge will, therefore, feel on its outer reaches a strong deformation field tending to produce an enstrophy cascade through stretching of the vortex material; no substantial effect will apply on the inward side. While it may be possible to contrive a vortex structure with strong deformation on the inside, all cases we have investigated are strongly asymmetric in this respect.

In more active situations, however, outside fluid apparently can be entrained into the main vortex. This is shown more clearly in Fig. 12, which is an enlargement of the final frame of Fig. 4 (i.e., at $t = 24$ d); note the entrainment of the "white" extravortex fluid into the main vortex. This entrainment takes place during merger of the main vortex with the secondary vortex shed during the earlier breaking event (see Fig. 4). Such behavior is common in vortex merger (e.g., Dritschel and McIntyre 1990).

e. *Kinematics inside and outside the vortex edge*

In order to reveal the character of the motion away from the vortex edge, a series of experiments was run with identical dynamics to some of those described above, but with additional contours prescribed at $t = 0$. These extra contours are dynamically passive, having no potential vorticity contrast across them, but act as tracers, being advected by the local flow in the same way as the dynamical contour. In the initial, undisturbed state these contours are circular and at radii $(0.25, 0.5, 0.75, 1.5)r_0$. The first set of experiments described next are for the nondivergent case $\gamma = 0$. As we shall see, the behavior in this case is rather different from that with nonzero γ.

Figure 13 shows a case with $H_0 = 0.12$, well below the breaking threshold. Although the potential vorticity contour does not break (in fact it remains quite smooth with no sharp curvature), the passive outer contour clearly does; its behavior is very similar to that shown by the potential vorticity contour with supercritical forcing. This example illustrates that vigorous material transport can occur outside the vortex even when the vortex itself is not breaking. The reason is, of course, that there is a stagnation point outside the vortex edge but near or inside the outer tracer contour. In fact, the outer region is so active that the material immediately outside the vortex edge is largely stripped off the vortex into the growing "tongue" of material entrained into the "westward" flow, leaving a more concentrated gra-

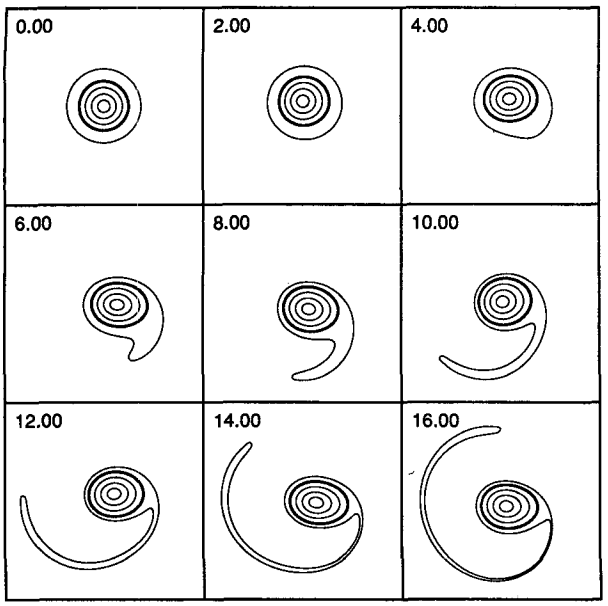

FIG. 13. Illustrating the kinematics of the nondivergent flow inside and outside the vortex edge. Contours are initially placed at radii 0.25, 0.5, 0.75, 1.00, and 1.50 r_0. All but the fourth of these (the darker one) are dynamically passive. This is a subcritical case, $H_0 = 0.12$.

dient of material contours just outside the vortex edge. This "vortex stripping" has been noted in other contexts (B. Legras and D. Dritschel, personal communication) while the steepening of gradients near the

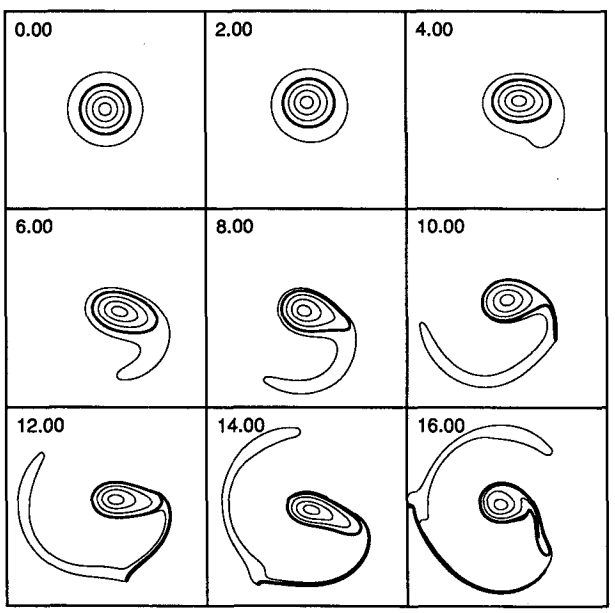

FIG. 14. As Fig. 13, but for a weakly supercritical case; $H_0 = 0.17$.

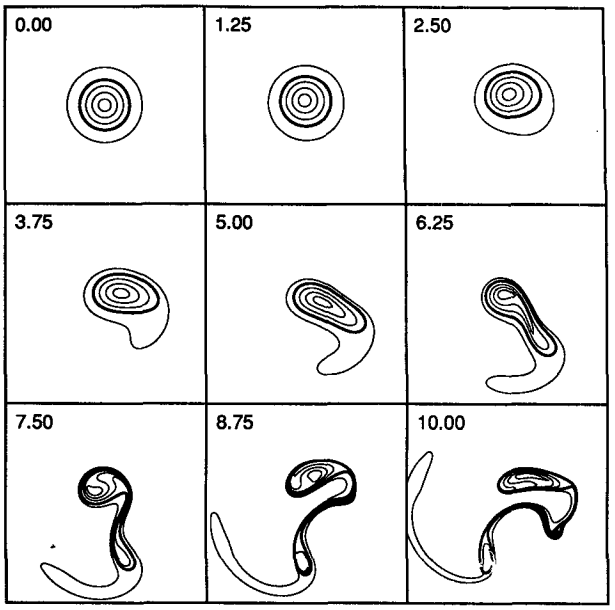

FIG. 15. As Fig. 13, but for a strongly supercritical case; $H_0 = 0.25$.

vortex edge has been emphasized by Juckes and McIntyre (1987).

Figure 14 shows the evolution of the four nested contours for a slightly supercritical case. The evolution is in fact quite similar to that of the previous example, except that the active region in which the contours are irreversibly deformed has moved inward, and now (since the breaking threshold has been crossed as the stagnation point has moved inside the vortex) encompasses the vortex edge. The inner regions of the vortex are unaffected (i.e., the inner contours suffer only reversible deformations). In this case the stripping is more complete and the outer regions of the vortex itself are stripped off the inner vortex. Contours at the vortex edge (and at the leading edge of the extruded filament) become even more concentrated than in the previous case. At stronger supercriticality (Fig. 15), the active region moves further inward, eventually ($t \approx 10$ d) affecting even the innermost contour. The concentration of material gradients at the vortex edge through the wave breaking is also particularly dramatic in the late stages.

These three experiments—the first, especially—also highlight an important difference between the dynamics of this single-contour vortex and that to be expected for an immature polar vortex of similar intensity but with a smoother potential vorticity gradient. In the latter case, stationary Rossby waves on the vortex would break in the outer regions even for arbitrarily weak forcing (as critical-layer theory demonstrates, the breaking zone collapsing onto the zero wind line as

$H_0 \to 0$), this process leading to the establishment of the mature vortex that is presupposed in our calculations. Indeed, the reason for the existence of a finite breaking threshold in these experiments is the finite distance between the discrete vortex edge and the zero wind line, so that a finite-amplitude wave is required to move the stagnation point and the associated material deformation all the way to the vortex edge.

In these nondivergent experiments, we thus find no evidence for mixing of the vortex interior. Irreversible deformation of initially circular material contours occurs only when the vortex as a whole is strongly disrupted. With nonzero γ, however, the behavior is different. Figure 16 shows a case with weak breaking for $\gamma = 2r_0^{-1}$ and $H_0 = 0.1$. (Note that the passive outer contour of Figs. 13–15 is not shown here.) The first frame shows the structure at 90 d, shortly after a very weak breaking event; although the vortex has already undergone two large-amplitude pulsations, the material contours have maintained their integrity.

During the time interval shown, however, the two innermost contours become buckled, leading to substantial material rearrangement in the vortex interior, while the outer region of the vortex remains unmixed. Thus, the material rearrangement in the interior is spatially separated from the dynamical breaking. Nevertheless, the two appear to be causally linked, since we have not observed interior mixing in the absence of breaking. The convoluted structure of the vortex interior at a later time is shown in Fig. 17. This behavior is quite different from the nondivergent case, where we saw that the inner vortex is disrupted only when the dynamical breaking is sufficiently strong to encompass the vortex interior. The unperturbed nondivergent velocity profile has constant angular velocity in the interior—a consequence of the uniform vorticity in the interior that we have presupposed—and thus zero strain (see Fig. 1). With nonzero γ, however, the angular velocity decreases inward, and the strain is nonzero inside the vortex. Hence, the entire vortex interior is robust to material deformations in the nondivergent case, but is less so at nonzero γ.

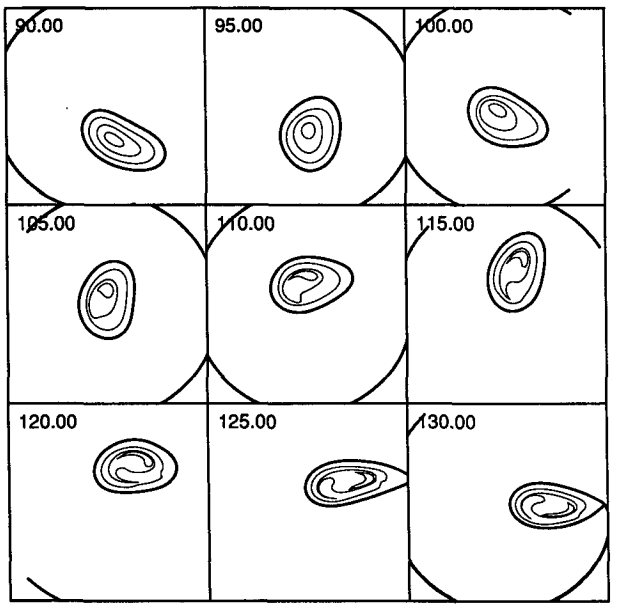

FIG. 16. Interior kinematics with finite Rossby deformation radius ($\gamma = 2$). Contours are initially placed at radii 0.25, 0.5, 0.75, and 1.0 r_0. All but the outer contour are dynamically passive. This is a very weakly supercritical case; $H_0 = 0.10$.

5. Summary

This investigation of the dynamics of a simple, perturbed f-plane vortex has revealed (not surprisingly, given the overall similarities of the systems studied) characteristics of Rossby wave breaking and of the concomitant ejection of material from the vortex similar to those evident in high-resolution, pseudospectral modeling studies of the stratospheric polar vortex (Juckes and McIntyre 1987; Juckes 1989). We have chosen here to restrict attention to a single-contour vortex, which in fact is a reasonable approximation to the mature polar vortex in middle and late winter, after the midlatitude potential vorticity gradient has been eroded through planetary wave breaking (McIntyre and Palmer 1983). In this case the vortex edge is a finite distance from the "zero wind line" and supercritical wave breaking occurs only if the height of the topography forcing the wave motion exceeds some finite threshold. When this threshold is not exceeded, the kinematic processes of deformation are still extant, as the tracer results of Fig. 13 show, but are sufficiently remote from the vortex edge not to disrupt its integrity. Thus, even when the vortex is not breaking, tracer distributions outside the vortex would be disrupted. Moreover, if there were a potential vorticity gradient in this region (weak enough not to impact much on the dynamics, say), this would also be destroyed, creating a mature, sharp-edged vortex (Juckes and McIntyre 1987).

With supercritical forcing the vortex edge becomes embroiled in the deformation field and the wave breaks; if the supercriticality is not too great, however, only the outer parts of the vortex are affected directly by the breaking at the vortex edge. In our nondivergent experiments, the inner regions, though perhaps distorted by the wave motion, remain intact in the presence of weakly supercritical breaking; only with strong supercriticality is the inner vortex disrupted. Experiments with finite Rossby radius, however, show three distinct regions: a core of material deformation, an intermediate relatively undisturbed annular region, and an outer region of wave breaking near the vortex edge.

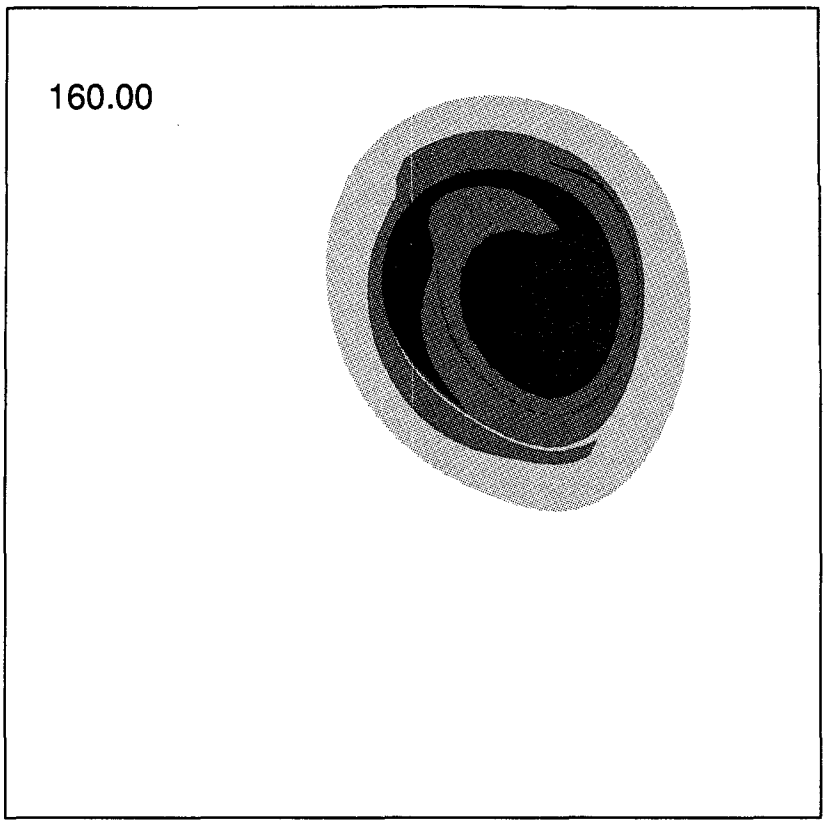

FIG. 17. Enlargement of the inner vortex structure for the case of Fig. 16 at a later time.

In fact, just as material deformations outside the vortex indicate how a sharp vortex edge would be formed, the inner vortex kinematics suggest that a second edge could be formed some way inside the vortex. In this context it is interesting to note (Schoeberl and Hartmann 1991, and references therein) that observations of various chemical species in and near the Antarctic polar vortex during the 1987 airborne mission revealed sharp gradients, not only at the vortex edge (as marked by a sharp isentropic gradient of potential vorticity), but also some 600 km inside the vortex (at the edge of the so-called "chemically perturbed region"). While there may be other explanations for this second boundary (it could be the boundary of the region where temperatures are cold enough to permit formation of polar stratospheric clouds; see Schoeberl and Hartmann 1991), the example of Fig. 17 suggests that there may be a dynamical explanation.

Evidently, the relative robustness of the vortex interior stems not only from the potential vorticity gradient at the vortex edge but from the structure of the flow inside the vortex. Of course, through the "invertibility principle" (Hoskins et al. 1985), the entire flow structure is implicit in the details of the potential vorticity contour. The point is that the occurrence or otherwise of material transport in any region is dependent not just on the dynamical rigidity of the vortex edge (through the familiar Rossby wave propagation mechanism) but also on sometimes subtle characteristics of the ambient flow field. One should be wary, therefore, of equating too literally the existence of a discrete barrier to material exchange with potential vorticity gradients alone.

The robustness of the vortex interior is also reflected in the asymmetry of the breaking. With the freedom that this technique affords we have confirmed the "onesidedness" found by Juckes and McIntyre whereby the breaking process leads to ejection of vortex air without any corresponding intrusion of outside material into the vortex. Again (as Juckes and McIntyre suggested) the reason for this seems to be the asymmetry of the vortex circulation with respect to the edge: the deformation field is much stronger outside than inside the edge. Over the wide range of parameters covered by our investigations we have found no example of inward breaking.

Though intrusion of material into the vortex does not occur during the breaking process, it does at times take place during remerger with secondary vortices shed earlier from the main vortex. During the merger, a

filament of outside material becomes entangled between the merging vortices and is entrained into the united main vortex. To the extent that these results may be applied to stratospheric dynamics, such intrusion might be expected in the northern stratosphere as the polar vortex is reestablished following a midwinter major warming (see Leovy et al. 1985); perhaps it might also occur during capture by the main vortex of debris ejected in less dramatic breaking events (examples of which are discussed by Clough et al. 1985), but we have seen no such examples in the current experiments.

We have distinguished here between supercritical breaking—the ejection of substantial amounts of material from the vortex—and what we have called microbreaking, which occurs in subcritical nondivergent cases. The distinction appears natural, given the sharp transition between these two classes of behavior. The latter process takes place at such small scale that it only occurs in our high-resolution experiments (and there seems to be little possibility of it being found in a conventional gridpoint or spectral model). Therefore, while some material is always eventually ejected in these experiments, the actual amount involved is extremely small in subcritical cases; so small, in fact, that its importance in the stratosphere is questionable. Indeed, the very existence of this phenomenon in the real stratosphere, in the presence of such influences as diabatic effects and straining by the vertical shear and by gravity wave motions, is open to doubt.

The material ejected from the vortex into the outer flow may exist either as filaments or as more bulky secondary vortices. In general, evolution into and between such structures is complex. At the point of ejection, a weak breaking event ejects a thin filament, while a stronger event will eject a "blob" of material. After ejection, a filament may roll up into small vortices, apparently through dynamic instability, although in strong "adverse" shear (Dritschel 1989b) or strain (Dritschel et al. 1991) it may in fact be stable and survive for some time. A secondary vortex may also be rather long lived, sometimes itself shedding filaments, sometimes capturing filaments, and, in some cases, being recaptured by the main vortex.

One aspect of the model results not evident in what has been presented here, but plainly apparent in animations, is the generation during breaking events of strong transient disturbances propagating along the vortex edge. The existence of these transients in situ is another reminder that, during active periods, stratospheric planetary waves cannot be viewed as simple linear extensions of tropospheric disturbances.

Overall, however, one should be cautious of equating too literally the behavior found in this simplified system with that of the stratospheric vortex. The aim of this study was to elucidate the range of behavior of this system in order to clarify the fundamental properties of perturbed vortices, to suggest processes that might occur in the stratosphere, and to aid interpretation of more realistic, but more restricted, high-resolution pseudospectral models of these phenomena.

Acknowledgments. We thank David Dritschel for generously providing the unforced version of the Contour Surgery code, Glenn Flierl and Darryn Waugh for useful discussions, and Michael McIntyre, whose thorough and insightful review of an earlier draft led to considerable improvements in revision. Some of the computations presented here were performed on the Cray-YMP at the Pittsburgh SuperComputing Center. This work was supported by the National Science Foundation through Grant ATM-9811459.

REFERENCES

Anderson, J. G., W. H. Brune, and M. H. Proffitt, 1989: Ozone destruction by chlorine radicals within the Antarctic vortex: the spatial and temporal evolution of ClO–O_3 anticorrelation based on in situ ER-2 data. *J. Geophys. Res.*, **94,** 11 465–11 479.

——, D. W. Toohey, and W. H. Brune, 1991: Free radicals within the Antarctic vortex: the role of CFCs in Antarctic ozone loss. *Nature,* **251,** 39–46.

Banner, M. L., and O. M. Phillips, 1974: On the incipient breaking of small scale waves. *J. Fluid Mech.*, **65,** 647–656.

Clough, S. A., N. S. Grahame, and A. O'Neill, 1985: Potential vorticity in the stratosphere derived using data from satellites. *Quart. J. Roy. Meteor. Soc.*, **111,** 335–358.

Deem, G. S., and N. J. Zabusky, 1978: Stationary V-states: interactions, recurrence and breaking. *Phys. Rev. Lett.*, **40,** 859.

Dritschel, D. G., 1988: The repeated filamentation of two-dimensional vorticity interfaces. *J. Fluid Mech.*, **194,** 511–532.

——, 1989a: Contour dynamics and contour surgery: numerical algorithms for extended, high resolution modelling of vortex dynamics in two-dimensional, inviscid compressible flows. *Computer Phys. Rep.*, **10,** 77–146.

——, 1989b: On the stabilization of a two-dimensional vortex strip by adverse shear. *J. Fluid Mech.*, **206,** 193–221.

——, and M. E. McIntyre, 1990: Does contour dynamics go singular? *Phys. Fluids A,* **2,** 748–753.

——, M. N. Juckes, P. H. Haynes, and T. G. Shepherd, 1991: The stability of a two-dimensional vorticity filament under uniform strain. *J. Fluid Mech.*, in press.

Haynes, P. H., 1989: The effect of barotropic instability on the nonlinear evolution of a Rossby wave critical layer. *J. Fluid Mech.*, **207,** 231–266.

Hoskins, B. J., M. E. McIntyre, and A. W. Robertson, 1985: On the use and significance of isentropic potential-vorticity maps. *Quart. J. Roy. Meteor. Soc.*, **111,** 877–946.

Juckes, M. N., 1989: A shallow water model of the winter stratosphere. *J. Atmos. Sci.*, **46,** 2934–2955.

——, and M. E. McIntyre, 1987: A high resolution, one-layer model of breaking planetary waves in the winter stratosphere. *Nature,* **328,** 590–596.

Leovy, C. B., C. R. Sun, M. H. Hitchman, E. E. Remsberg, J. M. Russell, L. L. Gordley, J. C. Gille, and L. V. Lyjak, 1985: Transport of ozone in the middle atmosphere: evidence for planetary wave breaking. *J. Atmos. Sci.*, **42,** 230–244.

McIntyre, M. E., 1987: Dynamics and tracer transport in the middle atmosphere: an overview of recent developments. *Transport*

Process in the Middle Atmosphere, G. Visconti and R. R. Garcia, Eds., Reidel, 267–296.

——, 1989: On the Antarctic ozone hole. *J. Atmos. Terr. Phys.,* **51,** 29–43.

——, and T. N. Palmer, 1983: Breaking planetary waves in the stratosphere. *Nature,* **305,** 593–600.

——, and ——, 1984: The "surf zone" in the stratosphere. *J. Atmos. Terr. Phys.,* **46,** 825–849.

——, and ——, 1985: A note on the general concept of wave breaking for Rossby and gravity waves. *Pure Appl. Geophys.,* **123,** 964–975.

Polvani, L. M., G. R. Flierl, and N. J. Zabusky, 1989a: Two-layer geostrophic vortex dynamics. Part I. Upper-layer V-states and merger. *J. Fluid Mech.,* **205,** 215–242.

——, N. J. Zabusky, and G. R. Flierl, 1989b: Filamentation of coherent vortex structures via separatrix crossing: a quantitative estimate of onset time. *The Physics of Fluids A,* **1,** 181–184.

Prather, M., and A. H. Jaffe, 1990: Global impact of the Antarctic ozone hole: chemical propagation. *J. Geophys. Res.,* **95,** 3473–3492.

Proffitt, M. H., D. W. Fahey, K. K. Kelly, and A. F. Tuck, 1989: High latitude ozone loss outside the Antarctic ozone hole. *Nature,* **342,** 233–237.

——, J. J. Margitan, K. K. Kelly, M. Loewenstein, J. R. Podolske, and K. R. Chan, 1990: Ozone loss in the Arctic polar vortex inferred from high-altitude aircraft measurements. *Nature,* **347,** 31–36.

Salby, M. L., R. R. Garcia, D. O'Sullivan, and J. Tribbia, 1990: Global transport calculations with an equivalent barotropic system. *J. Atmos. Sci.,* **47,** 188–214.

Schoeberl, M. R., and D. L. Hartmann, 1991: The dynamics of the stratospheric polar vortex and its relation to springtime ozone depletions. *Science,* **251,** 46–52.

——, L. R. Lait, P. A. Newman, and J. E. Rosenfield, 1991: The structure of the polar vortex. *J. Geophys. Res.,* submitted.

Stewartson, K., 1978: The evolution of the critical layer of a Rossby wave. *Geophys. Astrophys. Fluid Dyn.,* **9,** 185–200.

Warn, T., and H. Warn, 1978: The evolution of a nonlinear critical level. *Stud. Appl. Math.,* **59,** 37–71.

Waugh, D. W., and D. G. Dritschel, 1991: The stability of filamentary vorticity in two-dimensional geophysical vortex dynamics models, *J. Fluid Mech.,* submitted.